Applied Physics Letters PERSPECTIVE scitation.org/journal/apl

Self-trapping in bismuth-based semiconductors: Opportunities and challenges from optoelectronic devices to quantum technologies

Cite as: Appl. Phys. Lett. **119**, 220501 (2021); doi: 10.1063/5.0071763
Submitted: 16 September 2021 · Accepted: 15 November 2021 ·
Published Online: 2 December 2021

Sachin R. Rondiya,[1] Robert A. Jagt,[2] Judith L. MacManus-Driscoll,[2] Aron Walsh,[1,3] and Robert L. Z. Hoye[1,a)]

AFFILIATIONS

[1]Department of Materials, Imperial College London, Exhibition Road, London SW7 2AZ, United Kingdom
[2]Department of Materials Science and Metallurgy, University of Cambridge, 27 Charles Babbage Road, Cambridge CB3 0FS, United Kingdom
[3]Department of Materials Science and Engineering, Yonsei University, Seoul 120-749, South Korea

[a)]**Author to whom correspondence should be addressed:** r.hoye@imperial.ac.uk

ABSTRACT

Semiconductors based on bismuth halides have gained attention for a wide range of electronic applications, including photovoltaics, light-emitting diodes, and radiation detectors. Their appeal is due to their low toxicity, high environmental stability under ambient conditions, and easy processability by a wide range of scalable methods. The performance of Bi-based semiconductors is dictated by electron–phonon interactions, which limit carrier mobilities and can also influence optoelectronic performance, for example, by giving rise to a large Stokes shift for photoluminescence, unavoidable energy loss channels, or shallow optical absorption onsets. In this Perspective, we discuss the recent understanding of how polarons and self-trapped excitons/carriers form in Bi-based semiconductors (particularly for the case of $Cs_2AgBiBr_6$), their impact on the optoelectronic properties of the materials, and the consequences on device performance. Finally, we discuss the opportunities that control of electron–phonon coupling enables, including stable solid-state white lighting, and the possibilities of exploiting the strong coupling found in bipolarons for quantum technologies.

I. INTRODUCTION

Bismuth-based semiconductors have gained increased attention for optoelectronic applications, which, to a large extent, has been driven by the successes and limitations of lead-halide perovskites (LHPs).[1] LHP-based solar cells have demonstrated unprecedented increases in device efficiency and are now on the cusp of matching the record performance of crystalline silicon solar cells.[2,3] However, LHPs contain toxic lead, which is bioaccumulative and regulated in many jurisdictions.[4,5] This has prompted the search for materials that could replicate the exceptional optoelectronic properties of LHPs but without the same toxicity limitations, and these are known as "perovskite-inspired" materials or PIMs.[6,7] There have been three common types of PIMs investigated: (i) structurally analogous materials (i.e., which have a perovskite crystal structure such as $Cs_2AgBiBr_6$), (ii) chemically analogous materials (e.g., cesium bismuth iodide), and (iii) electronically analogous materials. The third group of PIMs includes compounds that are structurally and chemically dissimilar to LHPs (e.g., bismuth oxyiodide or BiOI)[8] but which share important features of the electronic structure of LHPs at band extrema. These features are mainly the hybridization of metal cation valence *s* and *p* orbitals with anion *p* orbitals to form bonding–antibonding states in the upper valence band, as well as an antibonding state in the conduction band minimum.[6]

Many of the PIMs considered have been compounds based on Bi^{3+} cations.[1] This is because Bi is next to Pb on the Periodic Table, and Bi^{3+} and Pb^{2+} are isoelectronic, possessing many electronic similarities, such that Bi-based compounds have been proposed to have the potential to replicate the ability of LHPs to tolerate point defects.[6] Defect tolerance occurs when the most common trap states are shallow with low capture cross sections, such that low non-radiative recombination rates occur despite high densities of defects.[9] This property has been one of the important factors behind the success of LHP photovoltaics.[10] Furthermore, Bi-based compounds have demonstrated no evidence of toxicity,[11] and many such compounds are stable in air.[1] The abundance of Bi is also sufficient for commercialization.[8] In addition, these materials can be processed by a wide range of

methods, from chemical vapor deposition (e.g., for BiOI)[12] to thin film solution processing (e.g., $Cs_2AgBiBr_6$ double perovskites)[13] and nanocrystal synthesis (e.g., $AgBiS_2$).[14]

However, exploration of Bi-based compounds for optoelectronics has not been straightforward. A critical complicating factor is the strong interactions between carriers and phonons in the lattice of many Bi-based PIMs (e.g., $Cs_3Bi_2I_9$, BiOI, or $Cs_2AgBiBr_6$), which lead to the mobility being reduced, in some cases severely reduced owing to carrier localization.[15–18] Furthermore, this carrier localization can result in an extra non-radiative loss channel that fundamentally limits the performance of optoelectronic devices.[19,20] However, in other cases, and in a positive sense, carrier localization can lead to radiative recombination with bright and broad luminescence, which can allow the materials to act as phosphors for white light emitting diodes.[21,22] Thus, the complete exploitation of bismuth-based semiconductors for optoelectronics will require in-depth understanding of how carriers/excitons interact with phonons and how these interactions can be controlled.

This Perspective discusses the recent fundamental insights into carrier–phonon coupling in Bi-based PIMs and the implications on their performance in optoelectronic devices. The scope and key points from this Perspective are illustrated in Fig. 1. We begin by briefly covering the key fundamentals to put the recent work in context. An understanding of carrier–phonon coupling in Bi-based semiconductors is only emerging, and the exact nature of these interactions remains an active area of debate, which we discuss. The impact of carrier–phonon coupling on the performance of photovoltaics and light-emitting diodes is then assessed, including both the detrimental effects that need to be mitigated as well as new opportunities. Finally, we discuss future routes to control carrier–phonon interactions, as well as new opportunities to exploit these interactions such as the possibility of using bipolarons for achieving photoinduced highly correlated states for quantum technologies.

II. CARRIER–PHONON INTERACTIONS

This section aims illustrating how the debate around carrier–phonon interactions in Bi-based PIMs for optoelectronics has recently evolved. To do this, we first begin by concisely describing some of the key concepts around carrier–phonon coupling, namely, how it influences the optoelectronic properties of materials and how the nature of carrier–phonon coupling is influenced by the electronic dimensionality of the material. An expanded discussion is provided in Sec. S1.1 of the supplementary material. We then discuss the literature on the specific case of $Cs_2AgBiBr_6$, which is the Bi-based PIM that has been the most extensively studied from the perspective of carrier–phonon coupling. This is to illustrate the debate and disagreements in the community, as well as how the understanding of the nature of carrier–phonon coupling in this material has evolved. These concepts can be more broadly applied to the wider family of Bi-based PIMs, which are discussed in more detail in Sec. S1.2 of the supplementary material.

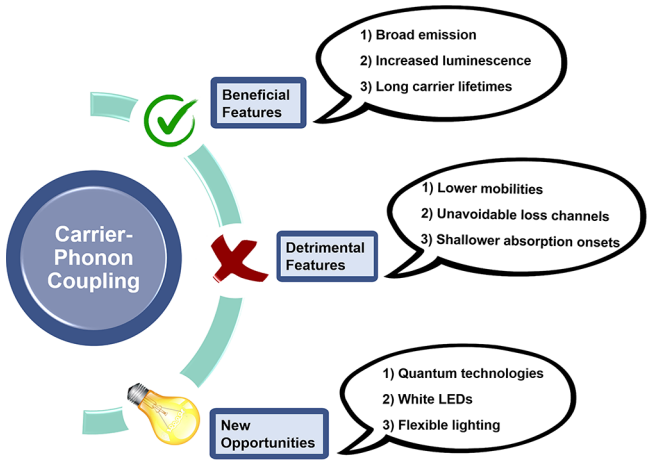

FIG. 1. Illustration of the scope of this Perspective on carrier–phonon coupling in bismuth-based perovskite-inspired materials, focusing on the beneficial and detrimental features along with the new opportunities opened up.

A. Fundamentals

The standard electronic band picture of semiconductors is depicted in an E vs k diagram [as shown in Fig. 2(a)], from which one can obtain insight into the carrier mobility from the effective mass and carrier recombination from the nature of the bandgap and the trap levels within the bandgap. However, carrier transport and recombination are also influenced by the thermal displacement of atoms from their equilibrium positions in the structure. In particular, atoms vibrate around their ideal crystallographic sites, and these quantized vibrations are described by phonons, which can be classified as optical or acoustic.[23] Optical phonons describe out-of-phase vibrations of adjacent atoms, whereas acoustic phonons describe vibrations from in-phase atomic displacements. In both cases, the vibrations can either occur perpendicular (transverse mode) or in-plane (longitudinal mode) to the direction of propagation.[22] Furthermore, structures are deformable, such that introducing a charge-carrier can result in the ionic lattice distorting around the carrier as it moves, which causes phonons to become coupled to the carrier, forming a polaron.[24,25] These interactions result in an increase in the effective mass, owing to the carrier dragging the distortion field around it as it moves. One of the most widely studied interactions between carriers and optical phonons in polar materials is the Fröhlich interaction, which involves longitudinal optical (LO) phonons. This is because Bi-based PIMs are polar crystals. When charge-carriers inside these materials couple to LO phonons, there is a variation in the interatom distance between adjacent ions, resulting in a fluctuation in energy and electric polarization.[26] Charge-carriers can also couple to acoustic phonons, and these result in shorter-range interactions that are often localized to one unit cell.[15,27–29] If this coupling to acoustic phonons is strong enough, the carrier can have severely reduced mobility, such that it is referred to as being "self-trapped." Polarons formed through the interaction between carriers and acoustic phonons are referred to as small polarons.[27,30] This contrasts to the polarons that form from Fröhlich interactions, which are more delocalized and referred to as large polarons.[15,31]

In addition to severely reducing the mobility of charge-carriers, carrier localization breaks down the electronic band picture shown in Fig. 2(a), resulting in a local polaronic picture, as depicted in the configuration coordinate diagram in Fig. 2(b). This diagram shows how the energy (E) of the lattice in the ground and excited states changes with local distortions (represented by coordinate Q) that can arise from interactions with LO or acoustic phonons and how carriers can localize into self-trapped states.[32] Emission from self-trapped states

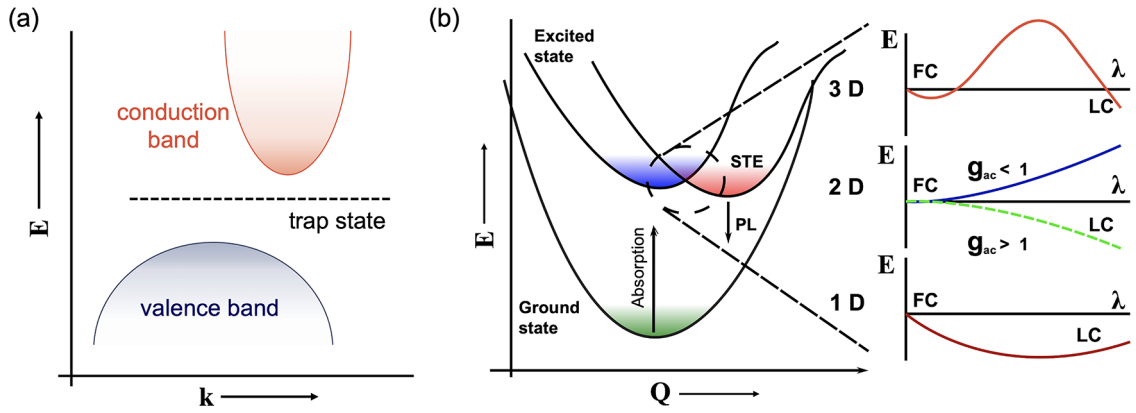

FIG. 2. (a) *E–k* diagram of a general material with a trap state. *E* is energy and k the wavevector. (b) General configuration coordinate diagram for a material that forms a self-trapped exciton (STE). *Q* is the configuration coordinate. Qualitative description of the dependence of the energy barrier for self-trapping on the dimensionless localization parameter λ for structurally 3D, 2D, and 1D materials. Here, FC refers to free carriers, LC refers to localized carriers, and g_{ac} denotes a dimensionless electron–phonon coupling parameter for acoustic phonons. Adapted with permission from Hoye *et al.*, Adv. Energy Mater. 2100499 (2021). Copyright 2021 Author(s), licensed under a Creative Commons Attribution (CC BY) license.

will give rise to luminescence that is often heavily Stokes-shifted to the optical bandgap (typically >100 meV).[33]

The propensity for materials to undergo self-trapping due to coupling to acoustic phonons is influenced by the dimensionality of the chemical bonding network, as shown in the inset of Fig. 2(b),[34] which depicts how the energy of the lattice in the excited state depends on the localization of the carrier wavefunction.[34] Here, $\lambda = a_0/a$, in which a_0 is the lattice parameter and a is a constant describing the radial extent of the carrier wavefunction. Thus, $\lambda = 1$ would imply that the carrier is localized to one unit cell, whereas in the other limiting case, when a tends toward infinity (and, therefore, $\lambda \rightarrow 0$), the carrier is unbound. It can be seen from Fig. 2(b), that for 3D structures, there is an energy barrier to localization, and this can allow both self-trapped and free carriers to co-exist, giving two photoluminescence (PL) peaks. Furthermore, when a barrier is present, self-trapping can only occur above certain temperatures.[16] The size of this energy barrier, W, depends on the characteristic frequency of the optical phonons (ω), reduced effective mass of the excitons (μ_{ex}), and the exciton–phonon coupling constant (γ), that is: $W \propto \omega^4/\mu_{ex}^3\gamma^4$.[34]

In contrast, in the 2D case, whether the lattice increases or decreases in energy as the carrier becomes more localized can be modeled in terms of an acoustic coupling factor, g_{ac}, which is given as

$$g_{ac} = \frac{E_d^2}{Ca_0} \cdot \frac{m}{3\pi\hbar^2}. \quad (1)$$

In Eq. (1), E_d is the acoustic deformation potential, C is the elastic constant of the material, m is the effective mass of the electron, and $\hbar$ is the reduced Planck's constant. E_d relates how changes in the volume of the material due to acoustic phonons lead to a change in the band positions of the material. When $g_{ac} > 1$, it is energetically favorable for self-trapping to occur because the energy of the system reduces for larger values of λ. Higher values of g_{ac} occur for materials with low elastic constants and high acoustic deformation potentials and are, therefore, readily observed in soft materials, which are common among Bi-based PIMs.[25,35] Within this model, no barrier to self-trapping occurs in lower-dimensional systems, regardless of the strength of coupling to acoustic phonons. Rather, free carriers or excitons (where $\lambda = 0$) are energetically unstable and will undergo localization (i.e., relax to a state where $\lambda > 0$, where the energy minimum occurs). Thus, the analysis shown in Fig. 2(b) explains why self-trapping becomes easier as dimensionality is reduced,[15] and the low electronic dimensionality of many Bi-based PIMs, therefore, make them prone to self-trapping. These fundamentals, and how they apply to Bi-based PIMs, are covered in greater detail in Sec. S1 of the supplementary material, particularly in Sec. S1.1.4. We refer readers to Refs. 15 and 34 for further discussion.

B. Carrier–phonon interactions in bismuth-based perovskite-inspired materials

As mentioned at the start of Sec. II, we keep the discussion of carrier–phonon interactions in Bi-based PIMs specific to the case of $Cs_2AgBiBr_6$, because this best illustrates the disagreements and difficulties in fully understanding the mechanism of how carriers and phonons interact. Discussion of carrier–phonon coupling in other Bi-based PIMs is given in Sec. S1.2 of the supplementary material, and some of the principles obtained from studies into $Cs_2AgBiBr_6$ can be applied to these other materials as well.

$Cs_2AgBiBr_6$ is a double perovskite (or elpasolite) that is comprised of alternating octahedra based on Ag^+ and Bi^{3+}. (More details are in Refs. 36–38.) Early work attributed carrier–phonon coupling in $Cs_2AgBiBr_6$ to be primarily Fröhlich[39–41] with carriers exhibiting band-like transport.[42] The latter observation was based on temperature-dependent pulse-radiolysis time-resolved microwave conductance (PRTRMC) measurements by Bartesaghi *et al.*, as represented in Fig. 3(a), which showed the sum of mobilities of all mobile carriers to increase as temperature decreases, consistent with reduced phonon scattering.[42] Measurements of the carrier scattering time, obtained from Drude–Smith fits to the frequency-resolved terahertz conductivity, exhibited a $T^{-0.5}$ dependence, which is also consistent with transport being dominated by large polarons.[40] The proposition that the dominant carrier–phonon couplings were mainly Fröhlich were also based on the temperature-dependence of the PL linewidth as shown in Fig. 3(b). In the weak coupling regime,[18] the full-width at

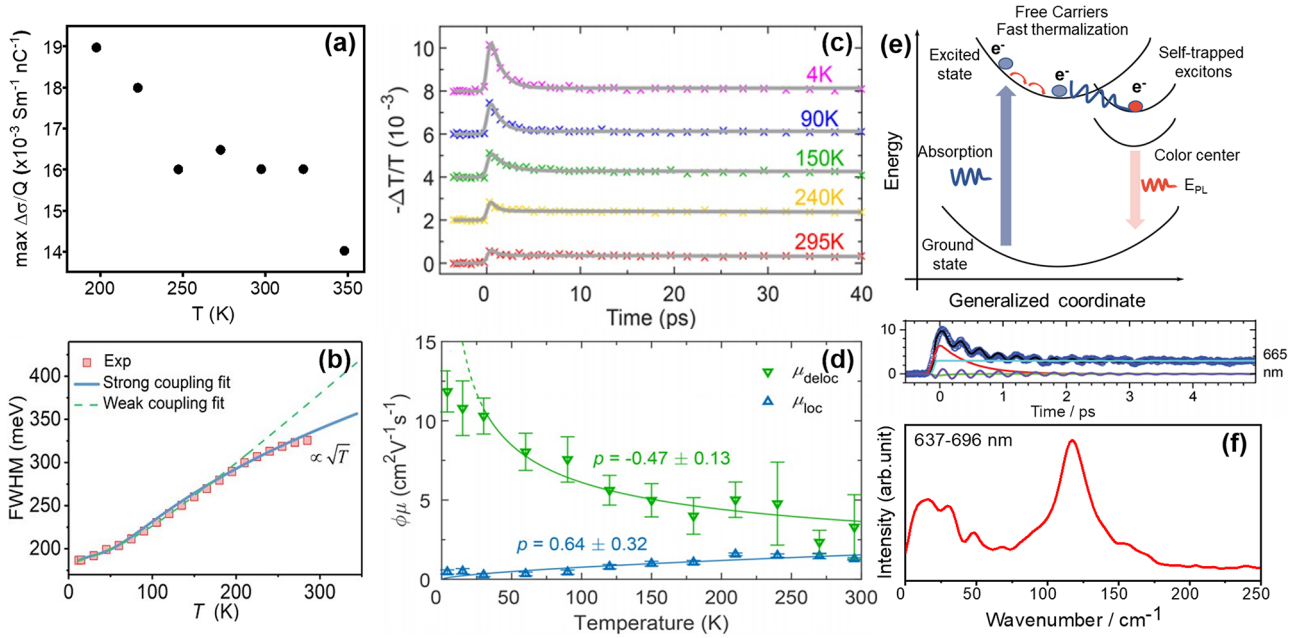

FIG. 3. (a) Maxima in the pulse-radiolysis time-resolved microwave conductance (PRTRMC) traces at different temperatures. Reproduced with permission from Bartesaghi *et al.*, J. Phys. Chem. C **122**, 4809 (2018). Copyright 2018 Author(s), licensed under a Creative Commons Attribution (CC BY-NC-ND) license. (b) PL linewidth of $Cs_2AgBiBr_6$ SC as a function of the temperature. Solid and dashed lines correspond to fitting with the conventional model for weak coupling and strong coupling, respectively. Reproduced with permission from Wu *et al.*, Sci. Adv. **7**, eabd3160 (2021). Copyright 2021 Author(s), licensed under a Creative Commons Attribution (CC BY-NC) license. (c) Optical pump terahertz probe (OPTP) photoconductivity transients for a $Cs_2AgBiBr_6$ thin film, measured at different temperatures under an excitation fluence of 10.1 μJ cm^{-2}. The transients at successively decreasing temperatures are offset vertically to aid visualization. The two-level charge-carrier mobility model was used to fit the data as represented by gray lines. (d) Temperature dependence of the effective charge-carrier mobilities associated with the delocalized (μ_{deloc}, green) and localized (μ_{loc}, blue) states in $Cs_2AgBiBr_6$ based on the OPTP measurements shown in part (c). The solid lines represent the relative change in $\phi\mu$ with respect to relative change in temperature in the corresponding colors with their exponents (p) displayed alongside. The data points for μ_{deloc} at the lowest two temperatures were not included in the plot, since the relative change is very small in that region indicated by the dashed green line. The mobilities are "effective" since the photon-to-charge branching ratio, ϕ, is not necessarily 1. Both parts (c) and (d) are reproduced with permission from Wright *et al.*, J. Phys. Chem. Lett. **12**, 3352 (2021). Copyright 2021 American Chemical Society. (e) Illustration of the proposed mechanism for self-trapping and luminescence from $Cs_2AgBiBr_6$ based on the discussion made in J. Phys. Chem. Lett. **12**, 3352 (2021)[17] and Sci. Adv. **7**, eabd3160 (2021).[18] (f) Kinetic decay in the transient absorption spectra of BiI_3 on mesoporous TiO_2, measured at 665 nm wavelength. The excitation wavelength was 400 nm. A Fourier transform was made on the oscillatory component of the kinetic decay curve, and this is shown in the bottom plot. Both plots are reproduced with permission from Scholz *et al.*, Phys. Chem. Chem. Phys. **20**, 10677 (2018). Copyright 2018 Royal Society of Chemistry.

half maximum (FWHM) of the PL peak (Γ) can be fit with the following equation:[39]

$$\Gamma = \Gamma_0 + \gamma_{ac} T + \gamma_{LO} n(T). \quad (2)$$

In Eq. (2), Γ_0 is a constant representing inhomogeneous broadening to the PL peak from scattering due to disorder or crystallographic imperfections. γ_{ac} is the acoustic phonon coupling constant, γ_{LO} is the LO phonon coupling constant, and n(T) is the occupation number of the LO phonon mode as a function of the temperature.[39] Several works have found γ_{LO} to be large with reported values in the range of 175–230 meV,[17,39,40,43] which substantially exceeds the γ_{LO} value for $MAPbI_3$ (40 ± 2 meV)[43] and $MAPbBr_3$ (58 ± 2 meV).[43] There is consensus in the literature that the dominant LO phonon mode carriers couple to are the A_{1g} symmetric stretching mode of $[BiBr_6]^{3-}$ octahedra, which has an energy of 175–180 cm^{-1} (~22 meV).[18,39,41,44] This has been found from both Raman measurements as well as Fourier transforms on the period of oscillations in the transient absorption kinetics in the picosecond timescale [similar to the example given for BiI_3 in Fig. 3(f)].[41,53]

While the γ_{LO} of $Cs_2AgBiBr_6$ exceeds that of $MAPbI_3$, the Fröhlich coupling constants are similar in the range of 2–3.[30,37,43] There is no direct correlation between γ_{LO} and the Fröhlich coupling constant α_{op} [refer to Eq. (S2), the supplementary material];[39] however, the values of α_{op} obtained would imply that Fröhlich interactions are in fact in the intermediate range for both materials.[45] Steele *et al.* noted that the values for α_{op} have primarily been determined through computations, which do not account for disorder between the Ag^+ and Bi^{3+} cations that may be prevalent, since the ionic radii for both cations are similar and the values of Γ_0 for $Cs_2AgBiBr_6$ are high (155–210 meV).[17,39,40] Despite the similarities in α_{op} between the two perovskites, $Cs_2AgBiBr_6$ has more limited mobilities, as well as broader PL FWHM than in $MAPbI_3$, which would not be explained if carrier–phonon coupling was limited to Fröhlich coupling alone. For example, the mobility calculated by Wu *et al.* from the α_{op} values using the Feynman–Osaka model for $Cs_2AgBiBr_6$ (27–33 cm^2 V^{-1} s^{-1}) is on the same order of magnitude as $CsPbBr_3$ (42–48 cm^2 V^{-1} s^{-1}) and just one order of magnitude below the calculated mobility of $MAPbI_3$ (94–197 cm^2 V^{-1} s^{-1}).[18] While $MAPbI_3$ and $CsPbBr_3$ single crystals have measured single-carrier mobilities in the range of 100–200 cm^2

V^{-1} s^{-1};[46,47] $Cs_2AgBiBr_6$ has a single crystal mobility of only 11.81 cm^2 V^{-1} s^{-1}.[48]

An alternative explanation is that coupling to acoustic phonons plays a significant role. In early works, this was considered unlikely because of the low value of γ_{ac} found from fitting using Eq. (2) (80–230 μeV K^{-1}).[39,40] However, it was recently pointed out by Wu *et al.* that Eq. (2) is only valid in the weak coupling regime, and when strong coupling occurs, as would be the case when acoustic phonons play a significant role, the PL linewidth would instead follow the equation:[18]

$$\Gamma = \Gamma_0 + \sqrt{\Gamma_A^2 + \Gamma_O^2}. \quad (3)$$

In Eq. (3), Γ_A and Γ_O are the PL line broadenings due to acoustic and optical phonons, respectively. With the expressions for Γ_A and Γ_O substituted in (refer to Ref. 18 for further details), Γ would overall vary as a function of $\sqrt{T}$, and fitting by Wu *et al.* recently found that this led to an improved fit to the PL FWHM, which would indeed suggest there to be strong coupling between carriers and phonons [Fig. 3(b)].[18]

Another objection[18] to carrier coupling to acoustic phonons raised in early works was that $Cs_2AgBiBr_6$ has a 3D structure and, therefore, should have a barrier to self-trapping [refer to Fig. 2(b) inset and the discussion in Sec. II A].[17] However, (i) the barrier to self-trapping in 3D systems is typically low compared to thermal energy at room temperature,[34] and (ii) the electronic dimensionality of $Cs_2AgBiBr_6$ is lower than 3D owing to the mismatch in orbitals from Ag and Bi contributing to the band-edges.[49] Calculations by Wu *et al.* found that the deformation potentials of $Cs_2AgBiBr_6$ (13.7 and 14.7 eV in the valence and conduction band extrema, respectively) are larger than those of $CsPbBr_3$ (2.2 and 6.3 eV for the valence and conduction band extrema, respectively), which would lead to a larger acoustic coupling constant [see Eq. (1)].[18] Disorder in the Ag–Bi sublattice may also lower the effective dimensionality of the system through the formation of inhomogeneous domains. Transient reflectance spectroscopy and optical pump teraherz probe (OPTP) measurements provide strong evidence in support of carrier trapping in $Cs_2AgBiBr_6$.[17,18] Transient reflectance spectroscopy shows there to be an initial ultrafast drop in the density of excited-state carriers, followed by a much slower decay,[18] which is consistent with previous short-time transient absorption spectroscopy measurements we took on this material.[44] The proposed explanation is that hot carriers thermalize via LO phonons on a sub-picosecond timescale before coupling to acoustic phonons on a <10 ps timescale and then interacting with defects on longer timescales. In support of this, Wu *et al.* found that changing the defect density of $Cs_2AgBiBr_6$ did not influence the kinetics on the <10 ps timescale.[18]

OPTP measurements also showed there to be rapid localization, in which the mobility of carriers rapidly decreased from 6.8 –12 cm^2 V^{-1} s^{-1} immediately after photo-excitation to 0.4 –1.3 cm^2 V^{-1} s^{-1} on a picosecond timescale [Fig. 3(c)].[17,18] Notably, the localization rate was found to be temperature-independent, which is consistent with self-trapping rather than trapping (refer to Sec. S1.1.5, supplementary material).[17] Furthermore, temperature-dependent measurements showed that carriers formed immediately after photo-excitation have a negative exponent of mobility with temperature (consistent with large polarons), whereas carriers after localization have a positive exponent (consistent with the thermally activated hopping of small polarons) as demonstrated in Fig. 3(d).[17] Wright *et al.* also argued that the rapid localization is not due to carrier relaxation to color centers (i.e., energy states in the bandgap that give rise to luminescence), because: (i) the final mobility of the localized state (1.3 cm^2 V^{-1} s^{-1} at room temperature) exceeds that expected from carriers tightly bound in traps; (ii) the trap density would need to be extremely high in order to localize carriers on the picosecond timescale; and (iii) carrier diffusion to color centers would be temperature-dependent, whereas the localization rate was found to not depend on the temperature.[17] Furthermore, recent measurements by us and others of the temperature-dependent field-effect mobility in $Cs_2AgBiBr_6$ are in agreement with these OPTP results, in which it was shown that when the effects of ion migration at grain boundaries are mitigated, the mobility exhibits a positive correlation with temperature, which is consistent with the thermally activated hopping of small polarons.[50] Overall, the proposed mechanism from Wu *et al.* and Wright *et al.*, illustrated in Fig. 3(e), is that carriers initially couple to LO phonons on a 0.2 ps timescale.[18] The strong distortion of the lattice within the large polaron then leads to coupling to acoustic phonons, thus forming small polarons or self-trapped carriers/excitons[18] with a timescale of 1.0–4.7 ps.[17,18] Subsequently, these localized states diffuse to color centers and undergo radiative recombination, giving PL that is broad and red-shifted to the optical bandgap.[17]

We note that an alternative explanation for the red-shifted PL is due to defect-bound excitons, which initially are associated with the direct transition, before undergoing intervalley scattering to the indirect bandgap. This process also depends on strong carrier–phonon coupling. This alternative explanation was provided by Dey *et al.* based on time-resolved PL spectra measurements of $Cs_2AgBiBr_6$ nanocrystals with a size of 8.9 ± 0.2 nm. Immediately after photoexcitation, the PL peak is centered at ∼2.9 eV, and this red-shifts by 1 eV within 10 ps–1.9 eV. The proposed mechanism is that initially the PL is due to a bound exciton, in which the hole is trapped in a shallow acceptor defect, such as an Ag^+ vacancy. Subsequently, the electron thermalizes from the X point to the L point of the Brillouin zone and is Coulombically bound to the trapped hole to form an exciton associated with the indirect bandgap.[51] In scattering from the X point to the L point, there is a reduction in the electron effective mass. On the one hand, this would lead to a reduction in the exciton E_b,[51] but on the other hand, this would also correlate with an increase in mobility, in which OPTP measurements show not to be the case.[17,18] Thus, analysis of OPTP measurements suggests that intervalley scattering does not occur.[17] Another matter of debate in the community is whether excitons initially form above the indirect bandgap at the direct transition. It is beyond the scope of this Perspective to discuss this, but the reader is referred to Refs. 17 and 52 for contrasting views on this topic, as well as Ref. 38 for further discussion.

Thus, the discussion above on the specific case of $Cs_2AgBiBr_6$ shows that elucidating the exact nature of carrier–phonon coupling in materials is not straightforward. While earlier works attributed carrier–phonon interactions to be Fröhlich, there is a growing body of evidence that the coupling of carriers to acoustic phonons plays a dominant role, leading to the formation of small polarons or self-trapped excitons. This accounts for the low mobilities found in this system, as well as these mobilities increasing with temperature. From the broader discussion of Bi-based PIMs in Sec. S1.2 in the

supplementary material, it can be seen that self-trapping has been found across the wider family of double perovskites, as well as many other Bi-based PIMs with low electronic dimensionality.

III. IMPLICATIONS OF CARRIER–PHONON COUPLING ON DEVICE PERFORMANCE

By modifying the band picture for semiconductors, carrier–phonon coupling can influence how charge-carriers transport within the material and undergo recombination. This section discusses the implications on the performance of bismuth-based PIMs in photovoltaic devices, as well as the new opportunities enabled in solid-state white-light emitting diodes.

A. Photovoltaic devices

1. Carrier transport

A photovoltaic device needs to not only absorb light but also transport photogenerated carriers to charge-selective contacts.[54] Historically, the development of solar materials has focused almost exclusively on the former property, but more recent efforts to design "defect-tolerant" PIMs have placed greater emphasis on the latter.[6] Both drift and diffusion depend on the mobility-lifetime product, but the screening of PIMs has primarily emphasized the measurement and maximization of charge-carrier lifetime[55–58] with the assumption that the mobility of carriers does not significantly vary between different semiconductors. However, when strong electron–phonon coupling occurs, this is not the case.

First, carrier–phonon coupling reduces the carrier mobility. As discussed in Sec. S1.1 of the supplementary material, the formation of polarons will lead to an increase in the effective mass [refer to Eq. (S3), the supplementary material].[25,34] As an example, for the case of $Cs_2AgBiBr_6$, computations on the effect of large polarons have shown that the maximum mobility is in the range of only 14–33 $cm^2\ V^{-1}\ s^{-1}$.[18,59] The carrier mobility will be further reduced if self-trapping occurs and becomes dependent on the thermally activated hopping of carriers between sites (refer to Sec. II B). Second, if carriers are strongly coupled to phonons, their coupling to defects is reduced, which can lead to longer charge carrier lifetimes through reduced carrier-defect scattering.[60–62] Thus, evaluating the transport properties of new Bi-based PIMs solely based on carrier lifetime may lead to a falsely positive view of its potential. For example, $Cs_2AgBiBr_6$ thin films have been found from transient absorption spectroscopy or time-resolved photoluminescence to have long charge-carrier lifetimes in the hundreds of nanoseconds to microseconds,[18,44] but their diffusion lengths are on the order of 100 nm or lower. This limits their short-circuit current densities, fill factors, and external quantum efficiencies in photovoltaic devices,[63] which ultimately limit their power conversion efficiencies to a maximum of only 2.84%, well below the optical limit in efficiency (7.92%).[64] We note, however, that while $Cs_2AgBiBr_6$ thin films have limited mobilities, their single crystal counterparts have diffusion lengths $>1\ \mu$m, as measured by stroboscopic scattering microscopy.[65]

These factors have contributed to the power conversion efficiency and short-circuit current density of bismuth-based PIMs being well below their theoretical limits as shown in Figs. 4(a) and 4(b). In contrast, lead-halide perovskites, which exhibit predominantly Fröhlich coupling and have significantly lower exciton binding energies, have reached closer to their theoretical limits.

2. Luminescence and non-radiative losses

Light emission is a critical property that should be maximized in order to achieve the best photovoltaic performance.[77,78] The loss in the open-circuit voltage (V_{OC}) due to non-radiative recombination is related to the external quantum efficiency for electroluminescence if the solar cell was operated as a light-emitting diode (η_{ext}), as given as[78]

$$V_{OC}^{cell} = V_{OC}^{rad} - 2.303\frac{k_B T_A}{q}\left|\log_{10}\eta_{ext}\right|. \quad (4)$$

In Eq. (4), V_{OC}^{cell} and V_{OC}^{rad} are the open-circuit voltage of the cell under operation and at the radiative limit, respectively, while k_B is Boltzmann's constant, T_A is the absolute temperature of the devices, and q is the elementary charge.[78] One of the main factors the value for η_{ext} depends on is the photoluminescence quantum efficiency (PLQE), which gives the fraction of all recombination events (measured externally to the film) that are radiative.[78–80] Reference 78 discusses the other parameters influencing η_{ext}.

Self-trapping can either lead to a reduction or increase in the PLQE of Bi-based PIMs. PLQEs (as well as charge-carrier lifetimes) can be reduced due to the localized carrier directly coupling to the ground state and releasing its excess energy in a multi-phonon emission process, which opens up a new non-radiative decay channel.[34] Furthermore, self-trapped carriers or excitons can be thermally excited away from their localized state to reach the ground state, where they can then undergo further non-radiative relaxation.[19] In this case, the degree of non-radiative recombination would decrease at lower temperatures.[19] $Cs_2AgBiBr_6$ was observed by Wu *et al.* to increase in the PLQE when the temperature was decreased from room temperature to 77 K, although this was attributed by the authors to defect deactivation and exciton formation.[18]

3. Absorption onset and open-circuit voltage losses

The steepness of the optical absorption onset is another parameter that influences losses in V_{OC}.[78] This is illustrated in Fig. 4(d), which plots the V_{OC} loss from the radiative limit as a function of the Urbach energy (E_U) for different band gaps. Losses increase as the Urbach energy increases, and this results from a higher dark current.

The Urbach energy describes the steepness of the optical absorption onset as given as

$$\alpha(h\nu) = \alpha_0 \exp\left(\frac{h\nu - E_g}{E_U}\right). \quad (5)$$

In Eq. (5), $\alpha(h\nu)$ is the absorption coefficient for different photon energies ($h\nu$) above the bandgap (E_g), and α_0 is the absorption coefficient at the bandgap. For the case where coupling to acoustic phonons plays a prominent role, the Urbach energy can be related to the acoustic coupling constant [g_{ac}, refer to Eq. (1)] by[34,81–83]

$$E_U \propto \frac{g_{ac}}{s}. \quad (6)$$

In Eq. (6), s is a constant, known as the steepness index.[82] It can be seen from Eq. (6) that increased acoustic coupling will result in a

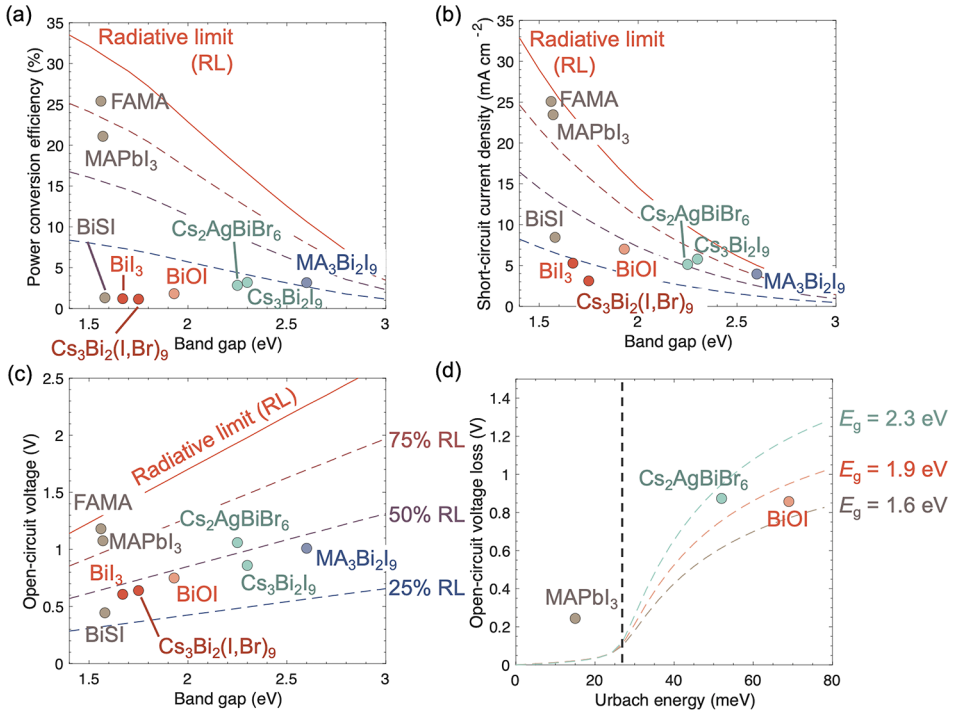

FIG. 4. Photovoltaic performance of bismuth-based perovskite-inspired materials compared to the performance of $[HC(NH_2)_2]_{0.73}[CH_3NH_3]_{0.27}Pb(Br_{0.008},I_{0.992})_3$ (FAMA) and $CH_3NH_3PbI_3$ ($MAPbI_3$) perovskites. (a) Power conversion efficiency, (b) short-circuit current density, and (c) open-circuit voltage of the devices compared to the radiative limits (RL), as well as 75%, 50%, and 25% of the RL. Note that the color coding of the RL lines is the same in (a)–(c), and these are labeled in part (c) only for clarity. The photovoltaic performance data are obtained from Refs. 8 and 66–74. (d) Open-circuit voltage loss against reported Urbach energy compared against the theoretical open-circuit voltage loss for different band gaps (E_g) if non-radiative losses due to the Urbach energy were the only loss process. The thermal energy at room temperature is marked with the dashed black line. The colors of the data points for the materials in (a)–(d) are based on the band gaps of the materials: ~1.6 eV (brown), 1.6–1.8 eV (red), 1.9 eV (pink), 2.2–2.3 eV (green), and 2.6 eV (blue). Details on the calculations of the radiative limits and losses can be found in Refs. 8, 11, and 12. The data on Urbach energy and open-circuit voltage loss are obtained from Refs. 8, 12, 44, 68, 75, and 76. Note that $Cs_2AgBiBr_6$ and BiOI have open-circuit voltage losses below those calculated owing to uncertainties in the Urbach energy of the film used in devices and the dark currents in the devices deviating from those calculated from the ideal blackbody spectrum. Nevertheless, this plot shows that the Urbach energies for both materials are strong contributors to their high open-circuit voltage losses.

shallower optical absorption onset (higher E_U), which, from Fig. 4(d), will lead to increased V_{OC} losses.[78,84]

The steepness of the optical absorption onset is also influenced by coupling to optical phonons, and this can be seen in the full expression for the Urbach energy or steepness parameter (refer to Refs. 81 and 85 for discussions), which depend on the optical phonon energy. From these expressions, stronger Fröhlich coupling will also lead to shallower optical absorption onsets. However, this is temperature-dependent, since at lower temperatures, the occupation of the dominant optical phonon mode will be reduced. The absorption onset, therefore, becomes steeper at lower temperatures.

4. Combined effects of carrier-phonon coupling on photovoltaic performance

Overall, increased coupling of charge carriers to phonons will lead to a reduction in photovoltaic performance because:

- There will be a reduction in carrier mobility, leading to a decrease in the drift and diffusion lengths. In turn, these will lead to a reduction in the short-circuit current density and fill factor, especially if the drift/diffusion length falls substantially below the thickness of the absorber. A reduction in mobility will also lead to a reduction in the V_{OC}, because at open-circuit, there is no internal field driving charge-separation by drift, and carrier extraction relies on diffusion. Thus, the dark current will increase, and the V_{OC} will decrease.
- There will be a reduction in PLQE in some cases, owing to the relaxation of carriers from self-trapped states to the ground state *via* multi-phonon emission processes. This will result in a reduction in the V_{OC}, as seen from Eq. (4).
- There will be a shallower optical absorption onset, leading to a reduction in the V_{OC} due to the increased dark current. Indeed, from Fig. 4(d), it can be seen that the V_{OC} loss of two example Bi-based PIMs, $Cs_2AgBiBr_6$ and BiOI, is primarily due to the high Urbach energies of these materials. In contrast, the $MAPbI_3$ perovskite has significantly lower Urbach energies, and the V_{OC} loss is then dominated by other factors. From the broader literature, these factors include defect states at interfaces and grain boundaries[86] or nanoscale heterogeneities,[87] which can all be addressed by changing the processing of the thin film or through passivation.[88,89] In contrast, the V_{OC} losses due to high Urbach energies arising from carrier–phonon coupling are intrinsic to

the material and cannot be overcome through processing changes alone.

The high propensity of Bi-based PIMs to couple to phonons, as well as their high exciton binding energies, contributes to their photovoltaic performance falling well below their radiative limits (Fig. 4). In particular, there are large voltage losses (from 100 meV up to >1 V) exhibited in these Bi-based PIMs [Fig. 4(c)]. Short-circuit current densities also fall below the 75% of the radiative limit mark [Fig. 4(b)]. While some of these effects will come about due to defect states forming in some of these materials that need to be addressed,[55] addressing the limitations arising due to carrier–phonon coupling will be critical to progress this field.

B. White-light emitters

In Sec. III A 2, it was explained how self-trapping can lead to a new non-radiative loss channel. Here, we explain how self-trapping can lead to increased luminescence that can be exploited in phosphors for white-light emission. Earlier, in Sec. II A, it was explained how carrier localization replaces the electronic band picture with the polaronic picture, and how this can be represented on a configuration coordinate diagram [Fig. 2(b) and also Fig. 5(a)]. Carriers in the self-trapped state can couple to the ground state, giving rise to photoluminescence, which is usually broad (refer to Sec. S1.1.3, the supplementary material, for further details). The strength of luminescence due to the coupling of the self-trapped carrier to the ground state could be larger than might be expected from free carriers/excitons in a periodic lattice. For example, $Cs_2AgBiBr_6$ has an indirect bandgap, which would normally limit the PLQE to low values <0.01%. However, it was found that PLQEs as high as 2% could be achieved from $Cs_2AgBiBr_6$ when excited in the bulk.[18]

This feature of self-trapping can be exploited in inorganic phosphors. In particular, if the PL peak can be tuned to emit in the visible wavelength range and span over a wide range of wavelengths, it can be excited by and mix with emission from a blue or standard UV-emitting GaN light-emitting diode (LED) to achieve white-light emission [idea illustrated in Fig. 5(a), inset]. For example, $Cs_2Ag_{0.60}Na_{0.40}InBr_6$ doped with 0.04% Bi (which was believed to improve the crystal quality) was found to emit with a broad PL peak spread over the entire visible wavelength range with a PLQE of $86 \pm 5\%$. When used as phosphor on GaN LEDs, Commission Internationale d'éclairage (CIE) coordinates of (0.396, 0.448) were obtained, which are within the range for white-light emitters, and these phosphors were stable under operation at 5000 cd m^{-2} luminance for 1000 h.[21] Broad, red-shifted PL has also been obtained in $Cs_3Bi_2X_9$[90] and $MA_3Bi_2X_9$.[91] In these two cases, the Br-based vacancy-ordered triple perovskites were used (which emitted in the blue wavelength range) and combined with a phosphor and GaN LED to give white-light emitting diodes. However, as the iodide fraction was increased, the PL peak became broader and its center red-shifted to the 500–600 nm wavelength range,[90,91] such that these materials may be used as phosphors themselves as represented in Fig. 5(b).

IV. FUTURE DIRECTIONS

From the discussion in this Perspective (particularly in Sec. II B on $Cs_2AgBiBr_6$ and Sec. S1.2, the supplementary material, on broader classes of Bi-based PIMs), it can be seen that strong carrier–phonon coupling is common in bismuth-halide-based PIMs to the extent that it has been labeled a "hallmark" of these materials.[41] This arises due to the soft, polar lattices, as well as the low electronic dimensionality in most materials explored thus far.[41] Despite its prevalence, awareness of this phenomenon is only beginning to emerge in the wider PIMs community, and there are disagreements in the field on the exact nature of carrier–phonon coupling. This is especially evident in the recent works on $Cs_2AgBiBr_6$, as discussed in Sec. II B. Moving forward, future exploration of Bi-based PIMs should focus on identifying whether Fröhlich coupling and self-trapping occur, which can be accomplished through optical pump terahertz probe (OPTP) spectroscopy, transient absorption spectroscopy (focusing especially on the sub-nanosecond timescale), and temperature-dependent spectrally resolved PL measurements, as well as other techniques that are covered in further detail in Refs. 15, 18, and 25. The deformation potential becomes an important consideration, which strongly influences the acoustic coupling [refer to Eq. (1)] and is one factor in determining if small polarons or self-trapped excitons will form.

A critical thrust in future efforts with Bi-based PIMs for photovoltaics is to understand how the loss channel due to self-trapping could be avoided. The aim will be to controllably change the configuration coordinate diagram to reduce non-radiative transfer to the ground state. Some hints on how this can be done from the discussion

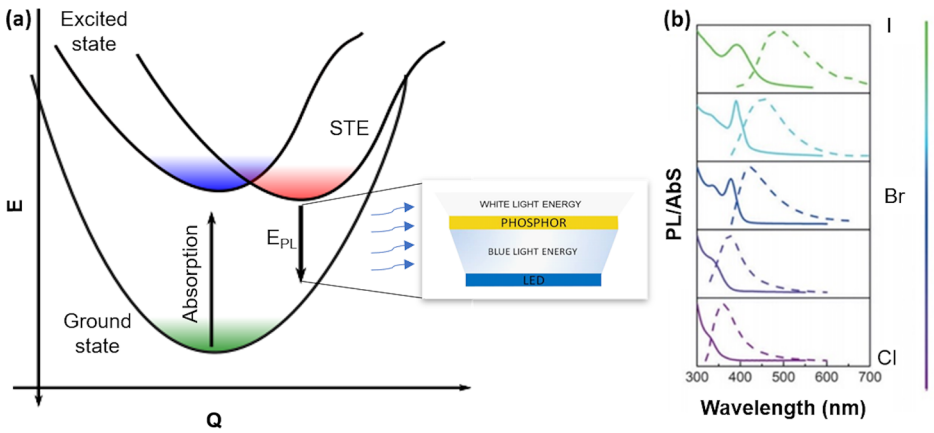

FIG. 5. (a) Illustration of how emission from the self-trapped state can be used for white-light emission. Here, blue light from a light-emitting diode (LED) is absorbed by the phosphor, exciting it from the ground (green) to excited (blue) state. The excited-state carriers then form self-trapped excitons (STEs), giving rise to broad emission over the visible wavelength range that combines with the blue light from the LED to give white light. (b) Shift in the photoluminescence spectra of $MA_3Bi_2X_9$ QDs when the halide is changed from Br to I. Reproduced with permission from Leng *et al.*, Angew. Chem. Int. Ed. **55**, 15012 (2016). Copyright 2016 Wiley.

in Sec. II A (with further details in Sec. S1.1, the supplementary material). That is, self-trapping can be avoided if the acoustic coupling constant is low (i.e., below a critical value of 1). From Eq. (1), it can be seen that this could be achieved in materials with stiffer lattices that are less deformable and have higher elastic constants. Furthermore, the acoustic phonons that are responsible for self-trapping can arise following the formation of large polarons. Thus, minimizing Fröhlich coupling constants could also be beneficial, and from Eq. (S2), the supplementary material, it can be seen that this can be achieved if: (i) the effective mass is lower, (ii) the phonon energy is larger, or (iii) the static and electronic dielectric constants are closer together. The first point can be achieved in materials with higher electronic dimensionality,[34] while the second point can be achieved in materials with lighter elements and stiffer bonds. The third point could be achieved in materials with lower ionicity, such as by pairing elements with lower absolute charges and electronegativities that are closer together. Finally, achieving materials that are electronically 3D can give rise to a barrier to self-trapping. Yet, as discussed earlier, these barriers are typically small compared to thermal energy, and self-trapping can, therefore, appear to be barrierless at room temperature. Increasing the characteristic phonon frequency will be beneficial, since the barrier to self-trapping scales to the fourth-power of this frequency.[34] Indeed, it would be instructive to measure the performance of photovoltaics at low temperatures. Not only would this reduce thermal energy to below the barrier to self-trapping in electronically 3D systems, but also it would depopulate the dominant phonon modes and, therefore, reduce or eliminate the effects of carrier–phonon coupling on device performance.

At the same time, it can be seen from the discussion in Sec. III B that self-trapping can be beneficial in creating a broad, radiative recombination channel with higher PLQEs than achievable from recombination across an indirect bandgap. This opens up the applicability of Bi-based PIMs for phosphors in white LEDs, where they have the advantage of being stable under ambient conditions and under continuous optical pumping. Tuning the PL peak energetic position and breadth will allow the color of the white LED to be tuned, and this may be achievable by tuning the composition of the Bi-based PIM to tune the bandgap, self-trapping energy, and deformation energy. Beyond further exploring the materials space, future efforts should also focus on achieving direct electrical injection into the self-trapped state, as has been recently demonstrated with low-dimensional tin-based perovskites.[92,93] This can allow the Bi-based PIMs to operate as white LEDs without the need for a GaN LED to act as a light source. This may lead to, for example, applications in flexible lighting, owing to the compatibility of the Bi-based PIM thin films with growth on polymer substrates.

Beyond light conversion in solar cells and LEDs, the same trapping phenomena discussed have utility in other application areas such as quantum technologies. In the ground-state, most bismuth-based semiconductors are diamagnetic; however, spin degrees of freedom can be activated upon illumination. Polarons formed of one carrier are paramagnetic spin $^1/_2$ centers, while self-trapped excitons often occur in the form of spin triplets. This provides a route to form transient localized spins in a semiconducting matrix. Under high illumination intensities, emergent behavior can manifest from the overlap of polaron wavefunctions. Indeed, due to the accessible Bi^{3+} and 5+ states, bipolarons can be formed, where a single Bi site exhibits negative-U behavior and traps two charge carriers, as in the oxide perovskite $BaBiO_3$ (refer to Sec. S1.1.6, the supplementary material for details on bipolarons).[74] $BaBiO_3$ in fact becomes metallic, then superconducting below 35 K, when hole doped with K.[94] Similar behavior may be accessible under illumination, which could give rise to photo-induced superconducting states such as those recently proposed in FeSe.[95] Superconducting behavior has been observed in other bismuth-based compounds such as bismuth oxysulfides.[96] The latest generation of Bi-based multi-component semiconductors offers fertile ground for discovering new classes of quantum materials.

SUPPLEMENTARY MATERIAL

See the supplementary material for complete discussion of the fundamentals of carrier–phonon coupling and the recent studies on carrier–phonon coupling in Bi-based PIMs beyond $Cs_2AgBiBr_6$. The supplementary material expands upon the discussion in Sec. II of the main text.

ACKNOWLEDGMENTS

S.R.R. and R.L.Z.H. would like to thank the Engineering and Physical Sciences Research Council (EPSRC; Grant No. EP/V014498/1). R.A.J. acknowledges support from a DTP studentship from EPSRC (Grant No. EP/N509620/1). R.A.J. and J.L.M.-D. would like to thank Bill Welland for financial support, as well as the Winton Programme for the Physics of Sustainability through the Pump-Prime scheme. J.L.M.-D. acknowledges support from the Royal Academy of Engineering Chair in Emerging Technologies (Grant No. CIET1819_24). R.L.Z.H. would like to thank the Royal Academy of Engineering through the Research Fellowships scheme (No. RF\201718\1701).

AUTHOR DECLARATIONS

Conflict of Interest

The authors declare no conflicts of interest.

DATA AVAILABILITY

Data sharing is not applicable to this article as no new data were created or analyzed in this study.

REFERENCES

[1]Y. T. Huang, S. R. Kavanagh, D. O. Scanlon, A. Walsh, and R. L. Z. Hoye, Nanotechnology **32**, 132004 (2021).
[2]See NREL National Renewable Energy Laboratory, https://www.nrel.gov/pv/cell-efficiency.html for "NREL Efficiency Chart" (2015) (accessed 24 September 2021).
[3]A. Polman, M. Knight, E. C. Garnett, B. Ehrler, and W. C. Sinke, Science **352**, aad4424 (2016).
[4]N. Moody, S. Sesena, D. W. deQuilettes, B. D. Dou, R. Swartwout, J. T. Buchman, A. Johnson, U. Eze, R. Brenes, M. Johnston, C. L. Haynes, V. Bulović, and M. G. Bawendi, Joule **4**, 970 (2020).
[5]J. Li, H.-L. Cao, W.-B. Jiao, Q. Wang, M. Wei, I. Cantone, J. Lü, and A. Abate, Nat. Commun. **11**, 310 (2020).
[6]R. E. Brandt, V. Stevanović, D. S. Ginley, and T. Buonassisi, MRS Commun. **5**, 265 (2015).
[7]A. M. Ganose, C. N. Savory, and D. O. Scanlon, Chem. Commun. **53**, 20 (2017).
[8]R. L. Z. Hoye, L. C. Lee, R. C. Kurchin, T. N. Huq, K. H. L. Zhang, M. Sponseller, L. Nienhaus, R. E. Brandt, J. Jean, J. A. Polizzotti, A. Kursumović,

M. G. Bawendi, V. Bulović, V. Stevanović, T. Buonassisi, and J. L. MacManus-Driscoll, Adv. Mater. **29**, 1702176 (2017).
[9]A. Walsh and A. Zunger, Nat. Mater. **16**, 964 (2017).
[10]E. M. Tennyson, T. A. S. Doherty, and S. D. Stranks, Nat. Rev. Mater. **4**, 573 (2019).
[11]R. Mohan, Nat. Chem. **2**, 336 (2010).
[12]R. A. Jagt, T. N. Huq, K. M. Börsig, D. Sauven, L. C. Lee, J. L. Macmanus-Driscoll, and R. L. Z. Hoye, J. Mater. Chem. C **8**, 10791 (2020).
[13]E. Greul, M. L. Petrus, A. Binek, P. Docampo, and T. Bein, J. Mater. Chem. A **5**, 19972 (2017).
[14]M. Bernechea, N. C. Miller, G. Xercavins, D. So, A. Stavrinadis, and G. Konstantatos, Nat. Photonics **10**, 521 (2016).
[15]L. R. V. Buizza and L. M. Herz, Adv. Mater. **33**, 2007057 (2021).
[16]L. R. V. Buizza, A. D. Wright, G. Longo, H. C. Sansom, C. Q. Xia, M. J. Rosseinsky, M. B. Johnston, H. J. Snaith, and L. M. Herz, ACS Energy Lett. **6**, 1729 (2021).
[17]A. D. Wright, L. R. V. Buizza, K. J. Savill, G. Longo, H. J. Snaith, M. B. Johnston, and L. M. Herz, J. Phys. Chem. Lett. **12**, 3352 (2021).
[18]B. Wu, W. Ning, Q. Xu, M. Manjappa, M. Feng, S. Ye, J. Fu, S. Lie, T. Yin, F. Wang, T. W. Goh, P. C. Harikesh, Y. K. E. Tay, Z. X. Shen, F. Huang, R. Singh, G. Zhou, F. Gao, and T. C. Sum, Sci. Adv. **7**, eabd3160 (2021).
[19]S. Yakunin, B. M. Benin, Y. Shynkarenko, O. Nazarenko, M. I. Bodnarchuk, D. N. Dirin, C. Hofer, S. Cattaneo, and M. V. Kovalenko, Nat. Mater. **18**, 846 (2019).
[20]C. H. Henry and D. V. Lang, Phys. Rev. B **15**, 989 (1977).
[21]J. Luo, X. Wang, S. Li, J. Liu, Y. Guo, G. Niu, L. Yao, Y. Fu, L. Gao, Q. Dong, C. Zhao, M. Leng, F. Ma, W. Liang, L. Wang, S. Jin, J. Han, L. Zhang, J. Etheridge, J. Wang, Y. Yan, E. H. Sargent, and J. Tang, Nature **563**, 541 (2018).
[22]W. Chu, Q. Zheng, O. V. Prezhdo, J. Zhao, and W. A. Saidi, Sci. Adv. **6**, eaaw7453 (2020).
[23]C. Franchini, M. Reticcioli, M. Setvin, and U. Diebold, Nat. Rev. Mater. **6**, 560 (2021).
[24]I. Kasik, J. Mrazek, O. Podrazky, M. Seidl, J. Aubrecht, P. Tobiska, V. Matejec, B. Kovacs, A. Markovics, M. Szili, and K. Vlckova, Mater. Sci. Eng., C **28**, 842 (2008).
[25]L. M. Herz, ACS Energy Lett. **2**, 1539 (2017).
[26]P. Y. Yu and M. Cardona, "Vibrational properties of semiconductors, and electron-phonon interactions," in *Fundamentals of Semiconductors*, Graduate Texts in Physics (Springer, Berlin/Heidelberg, 1996), pp. 107–158.
[27]R. T. Williams and K. S. Song, J. Phys. Chem. Solids **51**, 679 (1990).
[28]Y. Toyozawa, Prog. Theor. Phys. **26**, 29 (1961).
[29]F. X. Morrissey and S. L. Dexheimer, Phys. Rev. B **81**, 094302 (2010).
[30]A. M. Stoneham, J. Gavartin, A. L. Shluger, A. v. Kimmel, D. M. Ramo, H. M. Rønnow, G. Aeppli, and C. Renner, J. Phys.: Condens. Matter **19**, 255208 (2007).
[31]J. T. Devreese and A. S. Alexandrov, Rep. Prog. Phys. **72**, 066501 (2009).
[32]L. D. Whalley, P. van Gerwen, J. M. Frost, S. Kim, S. N. Hood, and A. Walsh, J. Am. Chem. Soc. **143**, 9123 (2021).
[33]Y. K. Jung, S. Kim, Y. C. Kim, and A. Walsh, J. Phys. Chem. Lett. **12**, 8447 (2021).
[34]R. L. Z. Hoye, J. Hidalgo, R. A. Jagt, J. Correa-Baena, T. Fix, and J. L. MacManus-Driscoll, Adv. Energy Mater. 2100499 (2021).
[35]C. W. M. Timmermans and G. Blasse, Phys. Status Solidi B **106**, 647 (1981).
[36]F. Wei, Z. Deng, S. Sun, F. Zhang, D. M. Evans, G. Kieslich, S. Tominaka, M. A. Carpenter, J. Zhang, P. D. Bristowe, and A. K. Cheetham, Chem. Mater. **29**, 1089 (2017).
[37]N. R. Wolf, B. A. Connor, A. H. Slavney, and H. I. Karunadasa, Angew. Chem. Int. Ed. **60**, 16264 (2021).
[38]H. Lei, D. Hardy, and F. Gao, Adv. Funct. Mater. 2105898 (2021).
[39]J. A. Steele, P. Puech, M. Keshavarz, R. Yang, S. Banerjee, E. Debroye, C. W. Kim, H. Yuan, N. H. Heo, J. Vanacken, A. Walsh, J. Hofkens, and M. B. J. Roeffaers, ACS Nano **12**, 8081 (2018).
[40]M. Keshavarz, E. Debroye, M. Ottesen, C. Martin, H. Zhang, E. Fron, R. Küchler, J. A. Steele, M. Bremholm, J. van de Vondel, H. I. Wang, M. Bonn, M. B. J. Roeffaers, S. Wiedmann, and J. Hofkens, Adv. Mater. **32**, 2001878 (2020).
[41]R. Kentsch, M. Scholz, J. Horn, D. Schlettwein, K. Oum, and T. Lenzer, J. Phys. Chem. C **122**, 25940 (2018).
[42]D. Bartesaghi, A. H. Slavney, M. C. Gélvez-Rueda, B. A. Connor, F. C. Grozema, H. I. Karunadasa, and T. J. Savenije, J. Phys. Chem. C **122**, 4809 (2018).
[43]A. D. Wright, C. Verdi, R. L. Milot, G. E. Eperon, M. A. Pérez-Osorio, H. J. Snaith, F. Giustino, M. B. Johnston, and L. M. Herz, Nat. Commun. **7**, 11755 (2016).
[44]R. L. Z. Hoye, L. Eyre, F. Wei, F. Brivio, A. Sadhanala, S. Sun, W. Li, K. H. L. Zhang, J. L. MacManus-Driscoll, P. D. Bristowe, R. H. Friend, A. K. Cheetham, and F. Deschler, Adv. Mater. Interfaces **5**, 1800464 (2018).
[45]J. M. Frost, Phys. Rev. B **96**, 195202 (2017).
[46]Z. Lian, Q. Yan, T. Gao, J. Ding, Q. Lv, C. Ning, Q. Li, and J. L. Sun, J. Am. Chem. Soc. **138**, 9409 (2016).
[47]J. Peng, C. Q. Xia, Y. Xu, R. Li, L. Cui, J. K. Clegg, L. M. Herz, M. B. Johnston, and Q. Lin, Nat. Commun. **12**, 1531 (2021).
[48]W. Pan, H. Wu, J. Luo, Z. Deng, C. Ge, C. Chen, X. Jiang, W. J. Yin, G. Niu, L. Zhu, L. Yin, Y. Zhou, Q. Xie, X. Ke, M. Sui, and J. Tang, Nat. Photonics **11**, 726 (2017).
[49]Z. Xiao, W. Meng, J. Wang, D. B. Mitzi, and Y. Yan, Mater. Horiz. **4**, 206 (2017).
[50]M. He, J. Huang, J. Li, J. S. Jang, U. P. Suryawanshi, C. Yan, K. Sun, J. Cong, Y. Zhang, H. Kampwerth, M. P. Suryawanshi, J. Kim, M. A. Green, and X. Hao, Adv. Funct. Mater. **31**, 2104528 (2021).
[51]A. Dey, A. F. Richter, T. Debnath, H. Huang, L. Polavarapu, and J. Feldmann, ACS Nano **14**, 5855 (2020).
[52]Z. Li, S. R. Kavanagh, M. Napari, R. G. Palgrave, M. Abdi-Jalebi, Z. Andaji-Garmaroudi, D. W. Davies, M. Laitinen, J. Julin, M. A. Isaacs, R. H. Friend, D. O. Scanlon, A. Walsh, and R. L. Z. Hoye, J. Mater. Chem. A **8**, 21780 (2020).
[53]M. Scholz, K. Oum, and T. Lenzer, Phys. Chem. Chem. Phys. **20**, 10677 (2018).
[54]R. Jaramillo, M. J. Sher, B. K. Ofori-Okai, V. Steinmann, C. Yang, K. Hartman, K. A. Nelson, A. M. Lindenberg, R. G. Gordon, and T. Buonassisi, J. Appl. Phys. **119**, 035101 (2016).
[55]R. E. Brandt, J. R. Poindexter, P. Gorai, R. C. Kurchin, R. L. Z. Hoye, L. Nienhaus, M. W. B. Wilson, J. A. Polizzotti, R. Sereika, R. Žaltauskas, L. C. Lee, J. L. Macmanus-Driscoll, M. Bawendi, V. Stevanović, and T. Buonassisi, Chem. Mater. **29**, 4667 (2017).
[56]R. E. Brandt, R. C. Kurchin, R. L. Z. Hoye, J. R. Poindexter, M. W. B. Wilson, S. Sulekar, F. Lenahan, P. X. T. Yen, V. Stevanović, J. C. Nino, M. G. Bawendi, and T. Buonassisi, J. Phys. Chem. Lett. **6**, 4297 (2015).
[57]A. H. Slavney, T. Hu, A. M. Lindenberg, and H. I. Karunadasa, J. Am. Chem. Soc. **138**, 2138 (2016).
[58]A. H. Slavney, L. Leppert, D. Bartesaghi, A. Gold-Parker, M. F. Toney, T. J. Savenije, J. B. Neaton, and H. I. Karunadasa, J. Am. Chem. Soc. **139**, 5015 (2017).
[59]J. Leveillee, G. Volonakis, and F. Giustino, J. Phys. Chem. Lett. **12**, 4474 (2021).
[60]F. Ambrosio, J. Wiktor, F. de Angelis, and A. Pasquarello, Energy Environ. Sci. **11**, 101 (2018).
[61]N. Österbacka, P. Erhart, S. Falletta, A. Pasquarello, and J. Wiktor, Chem. Mater. **32**, 8393 (2020).
[62]D. Manna, J. Kangsabanik, T. K. Das, D. Das, A. Alam, and A. Yella, J. Phys. Chem. Lett. **11**, 2113 (2020).
[63]G. Longo, S. Mahesh, L. R. V. Buizza, A. D. Wright, A. J. Ramadan, M. Abdi-Jalebi, P. K. Nayak, L. M. Herz, and H. J. Snaith, ACS Energy Lett. **5**, 2200 (2020).
[64]C. N. Savory, A. Walsh, and D. O. Scanlon, ACS Energy Lett. **1**, 949 (2016).
[65]M. Delor, A. H. Slavney, N. R. Wolf, M. R. Filip, J. B. Neaton, H. I. Karunadasa, and N. S. Ginsberg, ACS Energy Lett. **5**, 1337 (2020).
[66]C. A. R. Perini, T. A. S. Doherty, S. D. Stranks, J. P. Correa-Baena, and R. L. Z. Hoye, Joule **5**, 1024 (2021).
[67]J. J. Yoo, G. Seo, M. R. Chua, T. G. Park, Y. Lu, F. Rotermund, Y. K. Kim, C. S. Moon, N. J. Jeon, J. P. Correa-Baena, V. Bulović, S. S. Shin, M. G. Bawendi, and J. Seo, Nature **590**, 587 (2021).
[68]Z. Chen, B. Turedi, A. Y. Alsalloum, C. Yang, X. Zheng, I. Gereige, A. Alsaggaf, O. F. Mohammed, and O. M. Bakr, ACS Energy Lett. **4**, 1258 (2019).
[69]D. Tiwari, F. Cardoso-Delgado, D. Alibhai, M. Mombrú, and D. J. Fermín, ACS Appl. Energy Mater. **2**, 3878 (2019).

[70]D. Tiwari, D. Alibhai, and D. J. Fermin, ACS Energy Lett. **3**, 1882 (2018).
[71]B. bin Yu, M. Liao, J. Yang, W. Chen, Y. Zhu, X. Zhang, T. Duan, W. Yao, S. H. Wei, and Z. He, J. Mater. Chem. A **7**, 8818 (2019).
[72]Y. Han, H. Zhao, C. Duan, S. Yang, Z. Yang, Z. Liu, and S. Liu, Adv. Funct. Mater. **30**, 1909972 (2020).
[73]F. Bai, Y. Hu, Y. Hu, T. Qiu, X. Miao, and S. Zhang, Sol. Energy Mater. Sol. Cells **184**, 15 (2018).
[74]S. M. Jain, D. Phuyal, M. L. Davies, M. Li, B. Philippe, C. de Castro, Z. Qiu, J. Kim, T. Watson, W. C. Tsoi, O. Karis, H. Rensmo, G. Boschloo, T. Edvinsson, and J. R. Durrant, Nano Energy **49**, 614 (2018).
[75]X. Yang, Y. Chen, P. Liu, H. Xiang, W. Wang, R. Ran, W. Zhou, and Z. Shao, Adv. Funct. Mater. **30**, 2001557 (2020).
[76]A. Sadhanala, F. Deschler, T. H. Thomas, S. E. Dutton, K. C. Goedel, F. C. Hanusch, M. L. Lai, U. Steiner, T. Bein, P. Docampo, D. Cahen, and R. H. Friend, J. Phys. Chem. Lett. **5**, 2501 (2014).
[77]A. Polman and H. A. Atwater, Nat. Mater. **11**, 174 (2012).
[78]S. D. Stranks, R. L. Z. Hoye, D. Di, R. H. Friend, and F. Deschler, Adv. Mater. **31**, 1803336 (2019).
[79]N. Glück and T. Bein, Energy Environ. Sci. **13**, 4691 (2020).
[80]S. Sun, N. T. P. Hartono, Z. D. Ren, F. Oviedo, A. M. Buscemi, M. Layurova, D. X. Chen, T. Ogunfunmi, J. Thapa, S. Ramasamy, C. Settens, B. L. DeCost, A. G. Kusne, Z. Liu, S. I. P. Tian, I. M. Peters, J. P. Correa-Baena, and T. Buonassisi, Joule **3**, 1437 (2019).
[81]S. M. Wasim, G. Marín, C. Rincón, G. Sánchez Pérez, and A. E. Mora, J. Appl. Phys. **83**, 3318 (1998).
[82]M. Schreiber and Y. Toyozawa, J. Phys. Soc. Jpn. **51**, 1544 (1982).
[83]I. Studenyak, M. Kranjec, and M. Kurik, Int. J. Opt. Appl. **4**, 76 (2014).
[84]Y. Peng, T. N. Huq, J. Mei, L. Portilla, R. A. Jagt, L. G. Occhipinti, J. L. MacManus-Driscoll, R. L. Z. Hoye, and V. Pecunia, Adv. Energy Mater. **11**, 2002761 (2021).
[85]J. D. Dow and D. Redfield, Phys. Rev. B **5**, 594 (1972).
[86]M. Uller Rothmann, J. S. Kim, J. Borchert, K. B. Lohmann, C. M. O'Leary, A. A. Sheader, L. Clark, H. J. Snaith, M. B. Johnston, P. D. Nellist, and L. M. Herz, Science **370**, eabb5940 (2020).
[87]T. A. S. Doherty, A. J. Winchester, S. Macpherson, D. N. Johnstone, V. Pareek, E. M. Tennyson, S. Kosar, F. U. Kosasih, M. Anaya, M. Abdi-Jalebi, Z. Andaji-Garmaroudi, E. L. Wong, J. Madéo, Y. H. Chiang, J. S. Park, Y. K. Jung, C. E. Petoukhoff, G. Divitini, M. K. L. Man, C. Ducati, A. Walsh, P. A. Midgley, K. M. Dani, and S. D. Stranks, Nature **580**, 360 (2020).
[88]M. M. Byranvand and M. Saliba, Sol. RRL **5**, 2100295 (2021).
[89]J. Ye, M. M. Byranvand, C. O. Martínez, R. L. Z. Hoye, M. Saliba, and L. Polavarapu, Angew. Chem. Int. Ed. **60**, 21636 (2021).
[90]M. Leng, Y. Yang, K. Zeng, Z. Chen, Z. Tan, S. Li, J. Li, B. Xu, D. Li, M. P. Hautzinger, Y. Fu, T. Zhai, L. Xu, G. Niu, S. Jin, and J. Tang, Adv. Energy Mater. **28**, 1704446 (2018).
[91]M. Leng, Z. Chen, Y. Yang, Z. Li, K. Zeng, K. Li, G. Niu, Y. He, Q. Zhou, and J. Tang, Angew. Chem. Int. Ed. **55**, 15012 (2016).
[92]S. Li, J. Luo, J. Liu, and J. Tang, J. Phys. Chem. Lett. **10**, 1999 (2019).
[93]L. Lanzetta, J. M. Marin-Beloqui, I. Sanchez-Molina, D. Ding, and S. A. Haque, ACS Energy Lett. **2**, 1662 (2017).
[94]A. W. Sleight, Physica C **514**, 152 (2015).
[95]T. Suzuki, T. Someya, T. Hashimoto, S. Michimae, M. Watanabe, M. Fujisawa, T. Kanai, N. Ishii, J. Itatani, S. Kasahara, Y. Matsuda, T. Shibauchi, K. Okazaki, and S. Shin, Commun. Phys. **2**, 115 (2019).
[96]S. K. Singh, A. Kumar, B. Gahtori, Shruti, G. Sharma, S. Patnaik, and V. P. S. Awana, J. Am. Chem. Soc. **134**, 16504 (2012).